Acta Geotechnica
https://doi.org/10.1007/s11440-025-02773-x

RESEARCH PAPER

A finite strain thermal elastic visco-plastic consolidation model enhanced by particle swarm optimization of model parameters

Yang Liu[1,2] · Peichen Wu[2] · An Li[2] · Weiqiang Feng[3] · Zejian Chen[2] · Xudong Zhao[4] · Jun-Jie Zheng[5] · Jian-Hua Yin[1,6]

Received: 11 June 2025 / Accepted: 31 August 2025

Abstract

In this paper, a radial finite strain thermal consolidation model is extended to further consider the viscous behavior of soft soils. A newly developed thermal elastic visco-plastic (TEVP) constitutive model for the temperature and time-dependent stress–strain behavior of soft soils is implemented in a radial finite strain thermal consolidation model, which is solved through a numerical solver. This solving method is verified by comparing the calculated results by the numerical solver with two existing studies. After this, a particle swarm optimization (PSO) algorithm is employed to enhance the prediction performance of the proposed consolidation model by automatically calibrating the model parameters during the consolidation process. Two physical model tests were conducted to examine the validity of the proposed model and PSO-assisted method. The results indicate that the proposed radial consolidation model captures the viscous characteristics (including creep) of the time-dependent settlements of soft soils, which could not be simulated by the former reported models. The PSO-assisted method has demonstrated practical applicability when compared with physical model tests. The longer the observation time, the better the predictive performance of our radial finite strain thermal consolidation model. It is recommended that the observation time should not be shorter than the time required for primary consolidation.

Keywords Finite strain consolidation · Parameter calibration · Physical model test · PSO-assisted method · Thermal elastic visco-plasticity

✉ Jian-Hua Yin
cejhyin@polyu.edu.hk

Yang Liu
yang205.liu@polyu.edu.hk

Peichen Wu
peicwu@polyu.edu.hk

An Li
21071413r@connect.polyu.hk

Weiqiang Feng
fengwq@sustech.edu.cn

Zejian Chen
ze-jian.chen@connect.polyu.hk

Xudong Zhao
xzhaobl@connect.ust.hk

Jun-Jie Zheng
zhengjunjie@whu.edu.cn

[1] College of Civil and Transportation Engineering, Shenzhen University, Shenzhen 518060, China

[2] Department of Civil and Environmental Engineering, The Hong Kong Polytechnic University, Hong Kong 999077, China

[3] Department of Ocean Science and Engineering, Southern University of Science and Technology, Shenzhen, China

[4] Key Laboratory of Geotechnical Mechanics and Engineering of the Ministry of Water Resources, Changjiang River Scientific Research Institute, Wuhan, China

[5] School of Civil Engineering, Wuhan University, Wuhan 430074, China

[6] Department of Civil and Environmental Engineering, Research Institute of Land and Space, The Hong Kong Polytechnic University, Hong Kong 999077, China

Published online: 18 November 2025

1 Introduction

Prefabricated vertical drains (PVD) combined with vacuum preloading have been widely employed in soft ground improvement [4, 10, 11, 14, 15]. To further accelerate the consolidation process and enhance drainage efficiency, heating wires have been embedded into PVDs [31, 34], giving rise to the development of heated PVD technology, namely PVTD technology, shown in Fig. 1. Heat preloading reduces the viscosity of pore water and accelerates drainage [35], resulting in a markedly enhanced consolidation rate [8, 13].

A variety of constitutive models [1, 2, 6, 7, 12, 17, 21, 29, 32, 33] and theoretical investigations have been proposed to study the mechanisms involved in PVTD technology; among them, several thermo-hydro-mechanical (THM) models have been developed. For example, built on the thermal elastoplastic framework developed by Laloui and Cekerevac [21], recently, Lu et al. [28] introduced a nonlinear 1D thermal consolidation model; Liu et al. [25] developed a fully coupled axisymmetric large-strain thermal consolidation model; and Zhou et al. [37] presented the RTCS1 model, a large-strain thermal consolidation model established from the well-known RCS1 model established by Fox et al. [14], almost at the same time. These models effectively capture the coupled interactions among heat transfer, fluid flow, and mechanical deformation, as well as the temperature dependence of soil properties. While valuable, these models typically neglect the effect of viscous characteristics, a time-dependent deformation that is intrinsic to soft soils. Under external loading and elevated temperatures, time-dependent viscous behavior of soft soil can contribute significantly to long-term settlements and alter the rate of consolidation [23, 24, 36]. The experimental data in this paper also reveal that the soil exhibits obvious viscous characteristics. However, above-mentioned existing THM models neglect considering viscous characteristics of soft soils, which may limit their long-term prediction accuracy.

Moreover, most existing theoretical models are constrained to Class C level prediction, meaning that they are primarily interpretative and rely on fitting known data without predictive capacity beyond the observation period [22]. Heins and Grabe [16] and Losacco and Viggiani [27] indicated that Class C prediction needs artificially adjusted model parameters of a new proposed model or simulation to fit the known data. That is, this approach is carried out after the data are available, aiming to reproduce the data rather than forward prediction; hence, it is more accurately characterized as back analysis. This limitation hinders their practical utility in construction monitoring and post-treatment performance evaluation. To bridge the gap between academic modeling and engineering application, it is essential to develop a theoretical framework that not only

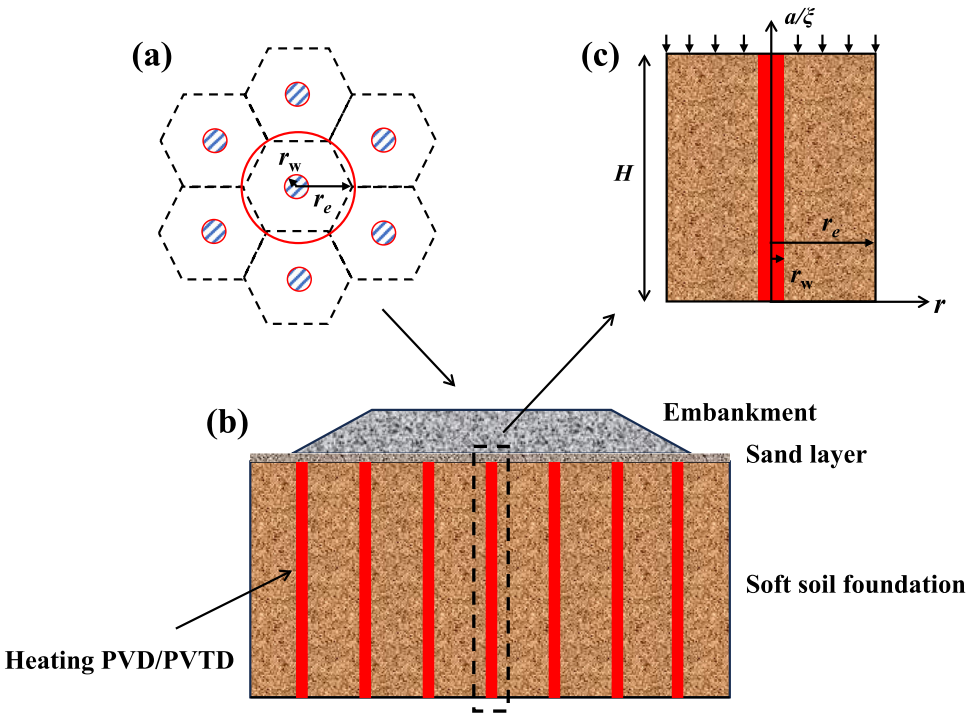

Fig. 1 Schematic diagram of heating PVD improved soft soils under embankment: **a** plane layout (triangular arrangement of PVTD), **b** cross section, and **c** unit cell

incorporates realistic soil behavior but also enables real-time forward prediction based on limited data.

In this study, a novel thermo-hydro-mechanical (THM) coupled consolidation model is proposed by incorporating viscous behaviors of soft soils into the existing THM framework [25]. A particle swarm optimization (PSO) algorithm proposed by Kennedy and Eberhart [20] is employed to enable the automatic identification of model parameters from limited experimental data. This approach allows the model not only to interpret past observations but also to reliably predict future consolidation behavior. To validate the proposed model and identification method, a carefully designed laboratory test was conducted. The results demonstrate the model's capability to capture the essential features of heat-assisted consolidation with viscous characteristics of soft soils and highlight its potential for practical engineering applications.

2 Evaluated model

2.1 Model establishment

To consider the temperature and time-dependent stress–strain behavior of soft soils, Chen and Yin [6] developed a one-dimensional constitutive model. The total strain rate can be expressed by Eq. (1), and more details can be referred to Chen and Yin [6] and are not repeated here.

$$\dot{\varepsilon}_z = \frac{\kappa_T}{V}\frac{1}{T}\frac{dT}{dt} + \frac{\kappa}{V}\frac{1}{\sigma'}\frac{d\sigma'}{dt} + \frac{\psi}{Vt_0}\exp\left[-\frac{V}{\psi}\left(\varepsilon - \varepsilon_{zp0}\right)\right] \cdot \left(\frac{\sigma'}{\sigma'_{zp0}}\right)^{\frac{\lambda}{\psi}} \cdot \left(\frac{T}{T_0}\right)^{\frac{\lambda_T}{\psi}} \tag{1}$$

in which T and T_0 denote the current and reference thermodynamic temperatures; σ' and σ'_{zp0} are the present effective stress and the soil's preconsolidation pressure, respectively, with ε_{zp0} being the corresponding strain on the reference time line at σ'_{zp0}. t_0 and t_e refer to the reference and equivalent times, while V is the specific volume. The normal compression and recompression behaviors are quantified by indices λ and κ, respectively, ψ_T is the creep coefficient accounting for temperature effects. κ_T captures the elastic response during cooling-reheating; and λ_T represents the virgin heating compression index.

By introducing the Terzaghi effective stress principle and transferring the thermodynamic temperature to degrees Celsius, Eq. (1) can be rewritten as

$$\frac{\partial\varepsilon}{\partial t} = \frac{\kappa_T}{V}\frac{\dot{T}}{T+273.15} + \frac{\kappa}{V}\frac{\partial(\sigma - u_w)/\partial t}{\sigma - u_w} + \frac{\psi}{Vt_0}\exp\left[-\frac{V}{\psi}\left(\varepsilon - \varepsilon_{zp0}\right)\right] \cdot \left(\frac{\sigma - u_w}{\sigma'_{zp0}}\right)^{\frac{\lambda}{\psi}} \cdot \left(\frac{T+273.15}{T_0+273.15}\right)^{\frac{\lambda_T}{\psi}} \tag{2}$$

where u_w is total pore pressure and σ is total stress.

Liu et al. [25] derived a radial finite strain consolidation model incorporating the thermal elastoplastic constitutive model proposed by Laloui and Cekerevac [21], and the strain rate of soil can be written as follows:

$$\frac{1}{r}\frac{\partial}{\partial r}\left(-\frac{k_r}{\rho_w g}\frac{1+e}{1+e_0}\frac{\partial u_w}{\partial r}\cdot r\right) + \frac{\partial}{\partial a}\left[-\frac{k_\xi}{\rho_w g}\left(\frac{1+e_0}{1+e}\frac{\partial u_w}{\partial a} - \gamma_w\right)\right] - a_v\frac{1+e}{1+e_0}\cdot\frac{\partial T}{\partial t} = \frac{\partial\varepsilon}{\partial t} \tag{3}$$

and

$$\begin{aligned} k_\xi(e,T) &= k_{\xi T_0}\cdot 10^{\frac{e-e_{zp0}}{C_{k\xi}}}\cdot\frac{\rho_{wT}\mu(T_0)}{\rho_{wT_0}\mu(T)}, k_r(e,T) \\ &= k_{rT_0}\cdot 10^{\frac{e-e_{zp0}}{C_{kr}}}\cdot\frac{\rho_{wT}\mu(T_0)}{\rho_{wT_0}\mu(T)} \\ \mu(T) &= -0.454\times10^{-3}\ln T + 2.349\times10^{-3} \end{aligned} \tag{4}$$

in which k_ξ and k_r are the hydraulic conductivities in the ξ- and r-directions, with their initial values of $k_{\xi T_0}$ and k_{rT0}, and C_{kr} and $C_{k\xi}$ are the corresponding permeability indices. ρ_{wT} and ρ_{wT_0} denote pore water density at the current and reference temperatures, respectively; $\mu(T)$ is the water viscosity; and γ_w its unit weight. The remaining symbols are total soil strain ε, the thermal expansion coefficient of saturated soft clay $\alpha_v(=(1-n)\alpha_s + n\alpha_w)$, and porosity n.

To further consider the viscous characteristics of soft soils, this paper extends the previous model [25] and incorporates the 1D TEVP model proposed by Chen and Yin [6]. The basic assumptions can be referenced from the previous study by Liu et al. [25]. Flow in fully saturated clay obeys to Darcy's law; pore water experiences no phase transition during consolidation; thermal equilibrium is maintained within the representative volume element, resulting in equal temperatures for pore water and particles; deformation is only occur in vertical direction (i.e., a-direction); and temperature changes have an insignificant impact on the density of soil particles. Based on these assumptions, and combining Eqs.(2) and (3), the governing equation can be expressed as

$$\frac{1}{r}\frac{\partial}{\partial r}\left(-\frac{k_r}{\rho_w g}\frac{1+e}{1+e_0}\frac{\partial u_w}{\partial r}\cdot r\right)+\frac{\partial}{\partial a}\left[-\frac{k_v}{\rho_w g}\left(\frac{1+e_0}{1+e}\frac{\partial u_w}{\partial a}-\gamma_w\right)\right]-a_v\frac{1+e}{1+e_0}\cdot\frac{\partial T}{\partial t}=\frac{\kappa_T}{V}\frac{\dot{T}}{T+273.15}+\frac{\kappa}{V}\frac{\partial(\sigma-u_w)/\partial t}{\sigma-u_w}+\frac{\psi}{Vt_0}\exp\left[-\frac{V}{\psi}\left(\varepsilon-\varepsilon_{zp0}\right)\right]\cdot\left(\frac{\sigma-u_w}{\sigma'_{zp0}}\right)^{\frac{\lambda}{\psi}}\cdot\left(\frac{T+273.15}{T_0+273.15}\right)^{\frac{\lambda_T}{\psi}} \tag{5}$$

By introducing a variable σ_{ah}, the Eq. (5) can be expressed as:

$$\begin{aligned}&\frac{\partial}{\partial a}\left[\frac{k_v}{\rho_w g}\left(\frac{1+e_0}{1+e}\frac{\partial u_e}{\partial a}\right)\right]+\frac{1}{r}\frac{\partial}{\partial r}\left(\frac{k_r}{\rho_w g}\frac{1+e}{1+e_0}\frac{\partial u_e}{\partial r}\cdot r\right)+a_v\frac{1+e}{1+e_0}\cdot\frac{\partial T}{\partial t}=-\frac{\kappa_T}{V}\frac{\dot{T}}{T+273.15}\\&-\frac{\kappa}{V}\frac{\partial(\sigma_{ah}-u_e)/\partial t}{\sigma_{ah}-u_e}-\frac{\psi}{Vt_0}\exp\left(\frac{e-e_{zp0}}{\psi}\right)\cdot\left(\frac{\sigma_{ah}-u_e}{\sigma'_{zp0}}\right)^{\frac{\lambda}{\psi}}\cdot\left(\frac{T+273.15}{T_0+273.15}\right)^{\frac{\lambda_T}{\psi}}\end{aligned} \tag{6}$$

with

$$\sigma_{ah}=\sigma-u_h,\ \frac{\partial\sigma_{ah}}{\partial a}=\frac{G_s-1}{1+e_0}\gamma_w \tag{7}$$

where σ_{ah} is the total stress above hydrostatic pressure; u_h is hydrostatic pore pressure; u_e is excess pore pressure, e is void ratio; and e_0 is initial void ratio.

The governing equation for energy conservation does not change when considering the 1D TEVP constitutive model; hence, this equation can be referred to Liu et al. [25] and presented as

$$\begin{aligned}&\left(\frac{C_s\rho_s(T_0)}{1+e_0}+\frac{C_w\rho_w(T)e}{1+e_0}\right)\frac{\partial T}{\partial t}=\frac{\partial}{\partial a}\left\{[\lambda_s(1-n)+\lambda_w n]\frac{1+e_0}{1+e}\frac{\partial T}{\partial a}\right\}\\&+\frac{1}{r}\frac{\partial}{\partial r}\left\{r\cdot[\lambda_s(1-n)+\lambda_w n]\frac{1+e}{1+e_0}\frac{\partial T}{\partial r}\right\}-C_w\rho_{wT}q_{w\xi}\frac{\partial T}{\partial a}-C_w\rho_{wT}q_{wr}\frac{1+e}{1+e_0}\frac{\partial T}{\partial r}\end{aligned} \tag{8}$$

with

$$v_{w\xi}=-\frac{k_v}{\rho_{wT}g}\frac{1+e_0}{1+e}\frac{\partial u_e}{\partial a},\quad v_{wr}=-\frac{k_r}{\rho_{wT}g}\frac{\partial u_e}{\partial r} \tag{9}$$

where C_w and C_s are the specific heat capacity of pore water and soil particles, respectively, and λ_w and λ_s are the thermal conductivity of pore water and soil particles, respectively.

Based on the characteristics of the proposed consolidation model, the initial and boundary conditions can also refer to the previous research of Liu et al. [25] as follows or based on actual boundary conditions.

$$\begin{aligned}&\text{initial conditions}: u_e(a,r,0)=\frac{G_s-1}{1+e_0}\gamma_w a\\&\text{(considering self - weight consolidation process)}\\&or\ u_e(a,r,0)=Q\\&\text{(loading after self - weight consolidation)},\\&T(a,r,0)=T_0\\&\text{boundary conditions for:}\\&\text{excess pore pressure}: \begin{cases}u_e(a,r_w,t)=-P(t)\\ \dfrac{\partial u_e(a,r_e,t)}{\partial r}=0\\ u_e(H,r,t)=0\\ \dfrac{\partial u_e(0,r_w,t)}{\partial a}=0\end{cases}\\&\text{temperature}: \begin{cases}T(a,r_w,t)=A(t)\\ T(a,r_e,t)+h\dfrac{\partial T(a,r_e,t)}{\partial r}=T_0\\ T(H,r,t)+h_1\dfrac{\partial T(H,r,t)}{\partial a}=T_0\\ T(0,r_w,t)+h_2\dfrac{\partial T(0,r_w,t)}{\partial a}=T_0\end{cases}\end{aligned} \tag{10}$$

where Q is external loading, h, h_1, and h_2 are heat-related boundary parameters, *and* $P(t)$, $A(t)$ are external time-dependent vacuum and heat preloadings, respectively, which have been introduced by Liu et al. [25].

2.2 Numerical implementation

The governing equations (i.e., Eqs. (6) and (8)) are highly nonlinear in space and time domains. It is therefore a challenge to give a reliable and robust analytical solution to the proposed governing equations. Considering this complexity, numerical solving tools are employed to calculate these equations. Several numerical solving tools are available for this task, and the COMSOL Multiphysics software is chosen to perform calculations. The soil domain is constructed within the COMSOL Multiphysics software utilizing the 2D axisymmetric modeling module, and the mesh is generated using the software's extra fine mesh setting. The governing equations are implemented using three coefficient form partial differential equation modules. This includes one module for the mass conservation equation (i.e., Eq. (6)), another for the energy conservation

equation (i.e., Eq. (8)), and a third module that implements the ordinary differential equation defined by the TEVP constitutive model in Eq. (2). Initial and boundary conditions are established in the coefficient form partial differential equation module in accordance with the actual boundary and initial conditions, followed by defining the simulation time span. The equations are subsequently solved utilizing the default solver (MUMPS solver) along with the standard solver parameters to achieve the simulations. All the calculation data are exported in the form of CSV or TXT format to conduct further analysis.

2.3 Verification of the numerical method

To verify the correctness and reliability of the numerical method, this section presents two verification examples comparing the proposed consolidation model with two existing consolidation models.

2.3.1 Verification with the RCS1 model

Fox et al. [14] once proposed a piecewise-linear model for a large-strain radial consolidation model, namely RCS1 model. This subsection employed the same parameters used in the RCS1 model to evaluate the numerical algorithm proposed in this paper. In order to compare with RCS1 model, the proposed consolidation model is degraded into a radial large-strain consolidation model under room temperature by setting the temperature of the heating PVD to room temperature and neglecting viscous characteristics of soft soils. The parameters for comparison are summarized by Fox et al. [14] and listed in Table 1.

The average degree of consolidation defined by the settlement is shown as follows:

$$U_s = \frac{\overline{S}_t}{\overline{S}_\infty} \tag{11}$$

Table 1 Parameters for model verification with Fox et al. [14]

Parameter	Value	Unit
H	10	m
r_w	0.05	m
r_e	0.5	m
G_s	2.7	–
e_{zp0}	2.1	–
$k_{\xi T_0}$	2×10^{-9}	m/s
k_{rT_0}	3×10^{-9}	m/s
λ	0.434	–
σ'_{zp0}	50	kPa
Q	50	kPa

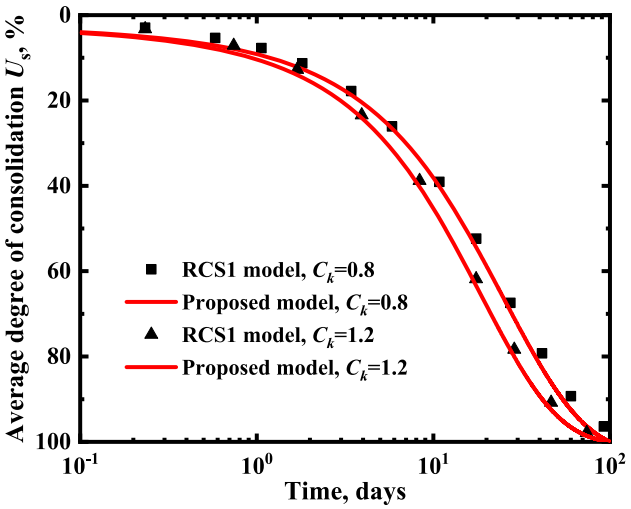

Fig. 2 The comparison of the average degree of consolidation and the results of Fox et al. [14]

in which $\overline{S}_t$ is average settlement at a given time t and $\overline{S}_\infty$ is average settlement at the end of consolidation.

Figure 2 compares the average degree of consolidation obtained from the RCS1 model and the proposed degraded model. It can be observed that the greater value of C_k, the faster the consolidation speed, and the greater the average degree of consolidation. The reason is that a greater C_k results in greater hydraulic conductivity at a given void ratio, thereby accelerating the consolidation rate. The average degree of consolidation calculated from the proposed numerical method shows a good agreement with the results from the well-established RCS1 model, which illustrates the correctness and reliability of the proposed numerical method.

2.3.2 Verification with large-strain radial consolidation model

Indraratna et al. [18] presented a finite element simulation for a large-strain radial consolidation model considering the nonlinear compressibility and permeability properties

Table 2 Parameters for model verification with Indraratna et al. [18]

Parameter	Value	Unit
r_w	0.1	m
r_e	1	m
e_{zp0}	1.5	–
k_{rT_0}	1×10^{-8}	m/s
λ	0.217	–
C_{kr}	0.75	–
σ'_{zp0}	50	kPa

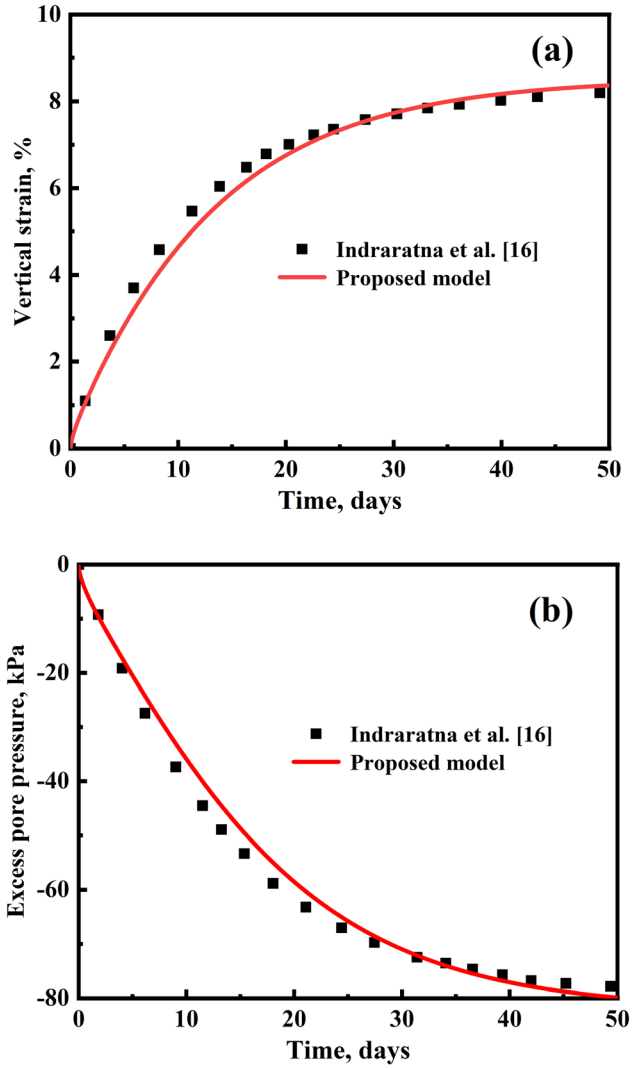

Fig. 3 The comparison of the proposed model with Indraratna et al. [18]:**a** vertical strain and **b** excess pore pressure

of soft clays. For ease of comparison, this subsection compares the calculation results from the proposed consolidation model by setting the temperature of the heating PVD to room temperature and neglecting viscous characteristics of soft soils against the results from ABAQUS simulations by Indraratna et al. [18]. The parameters used for comparison are summarized by Indraratna et al. [18] and listed in Table 2. The vacuum pressure of −80 kPa was applied at $t = 0$ and remained constant thereafter.

Figure 3 compares the results calculated from the proposed numerical method with the finite element simulations conducted by Indraratna et al. [18]. It can be found that the calculation results obtained from the numerical method proposed in this paper have good consistency with the previous simulations. The good agreement further confirmed the reliability of the proposed numerical method.

3 Methods for enhancing predictive capacity

Some existing predictive models primarily adopt Class C methods, where the analytical model is first developed and subsequently fitted to complete sets of post-construction data, such as settlement and excess pore water pressures. Although these methods can reasonably describe observed consolidation behaviors retrospectively, their heavy dependence on extensive historical datasets severely limits their predictive capability and practical utility in real-time monitoring and post-treatment evaluation scenarios. Moreover, certain parameters, for example, parameters $C_{k\xi}$ and $k_{\xi T_0}$ in the relationship between void ratio and permeability (e-k) under very low effective stresses, cannot be obtained through standard oedometer tests, or they require specialized equipment beyond the reach of most practitioners. To address both the data dependence of Class C prediction and the impracticality of bespoke apparatus, this study treats these difficult-to-measure coefficients as unknowns and determines them by combining limited field or laboratory observed data with a proposed consolidation model and basic parameters (e.g., void ratio, specific gravity, etc.) from simple bench-scale tests. The estimated values are then being input into the analytical consolidation model, facilitating forward predictions of future soil consolidation behavior. The whole process of obtaining unknown parameters can be regarded as an optimization task. The main goal is to achieve the global optimal solution of the fitness function (described in the following step (2)) using the measured data with the calculated data.

Particle swarm optimization is a swarm intelligence method that emulates the patterns and collaboration of avian flocking behavior to identify optimal solutions. In the application of PSO algorithm in geotechnical engineering, Cheng et al. [9] presented enhanced discontinuous-flying PSO variants to handle the non-circular failure surfaces problem. Ahmadi-Nedushan and Varaee [3] utilized PSO algorithm to minimize both cost and weight of reinforced concrete retaining walls. Kashani et al. [19] employed the algorithm to optimize footing dimensions for shallow foundations. Each particle, characterized by its position and velocity, is modified according to its current best position and the swarm's historical best position. In each iteration, particles reposition themselves in pursuit of a superior solution. The process persists until the specified number of iterations is fulfilled or a satisfactory solution is identified. In employing the PSO method, users need merely to configure essential variables, including population size, also called swarm size, and maximum iteration number. These two variables are crucial and can influence the optimization outcomes. The swarm size influences the

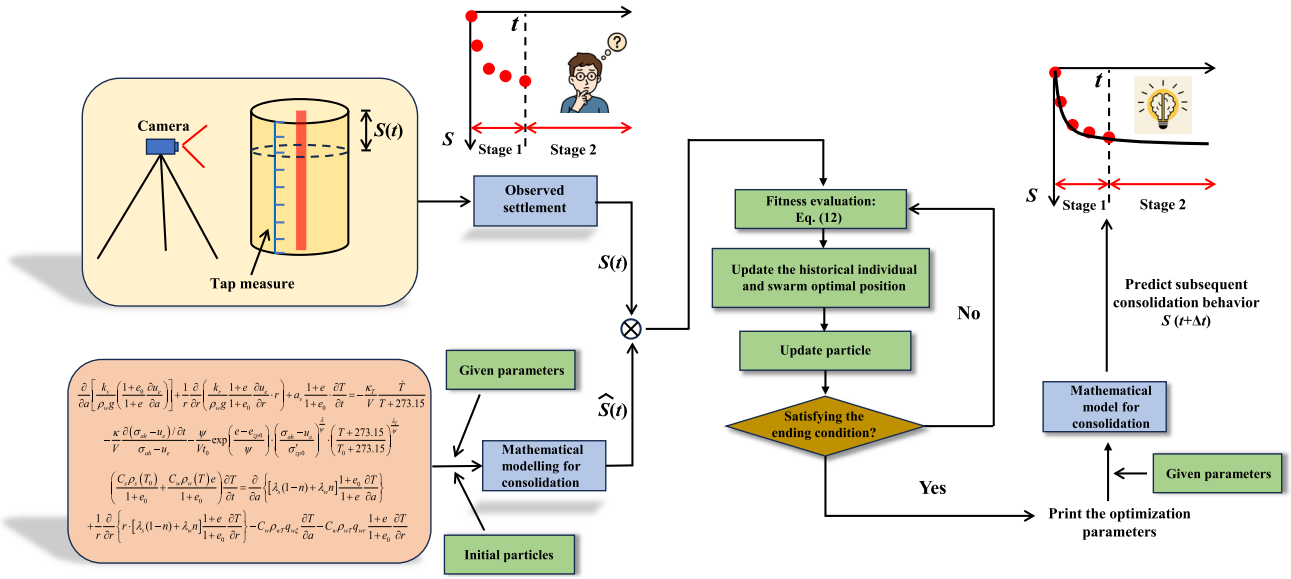

Fig. 4 Flowchart of PSO-assisted finite strain thermal consolidation prediction method

computational costs, while the number of maximum iterations influences both the convergence rate and the precision. The specific illustration of determing these two variables are provided in Sect. 5. To make the whole process clear and easier for engineers to use, detailed steps plotted in Fig. 4 are illustrated in the following:

(1) Collect measured data from the beginning of consolidation to a certain time (i.e., $S(t)$), say 10 days or 20 days, and conduct conventional geotechnical tests (e.g., oedometer test) to obtain basic physical and mechanical parameters of soil. The empirical values of soil can also be added together as another source of given parameters. At the same time, determine the parameters that need to be identified (usually taking the parameters that are difficult to determine) in the established mathematical model. Give the initial guess of these parameters in a reasonable range (this operation is shown in the following application case) and calculate the settlement (i.e., $\hat{S}(t)$) of soil using given and guessed parameters during the above-mentioned limited observed time, followed by transferring the calculation data from COMSOL to MATLAB software to evaluate the following fitness function (also called total error):

$$f = \sum_{j=1}^{k} \sum_{i=1}^{l} \left[s_i(T_j) - \hat{s}_i(T_j) \right]^2 \tag{12}$$

where S and $\hat{S}$ represent the measured and calculated soil settlement during the observation period, respectively.

(2) Check whether the convergence criteria (reaching maximum iteration number or minimum fitness function value) are satisfied. If so, the calculation terminates immediately. If not, these parameters to be identified are automatically adjusted according to the basic principle of the PSO algorithm. Then, a new set of parameters (including given parameters and optimized parameters) is sent to COMSOL for a new round of calculation. After several rounds of iteration, the fitness function reaches a global small value, followed by the termination of the whole optimization process and printing the optimized parameters.

(3) After obtaining the optimization parameters, a COMSOL calculation with given and optimized parameters is then performed to calculate the subsequent consolidation behavior (i.e., the time after observation).

4 Application of the proposed method in physical model testing

Two physical model tests on Hong Kong marine deposits (HKMD), incorporating self-weight and viscous characteristics of soft soils, were conducted and labeled Test 1 and Test 2. As shown in Fig. 5, each test used a 100-cm-tall acrylic column with a 40 cm inner diameter and a centrally installed copper tube (100 cm long, 0.75 cm radius). The upper end of the tube was connected via a PVC conduit wrapped in isothermal film to a water-bath heating system driven by a pump. Test 1 proceeded without heating (room

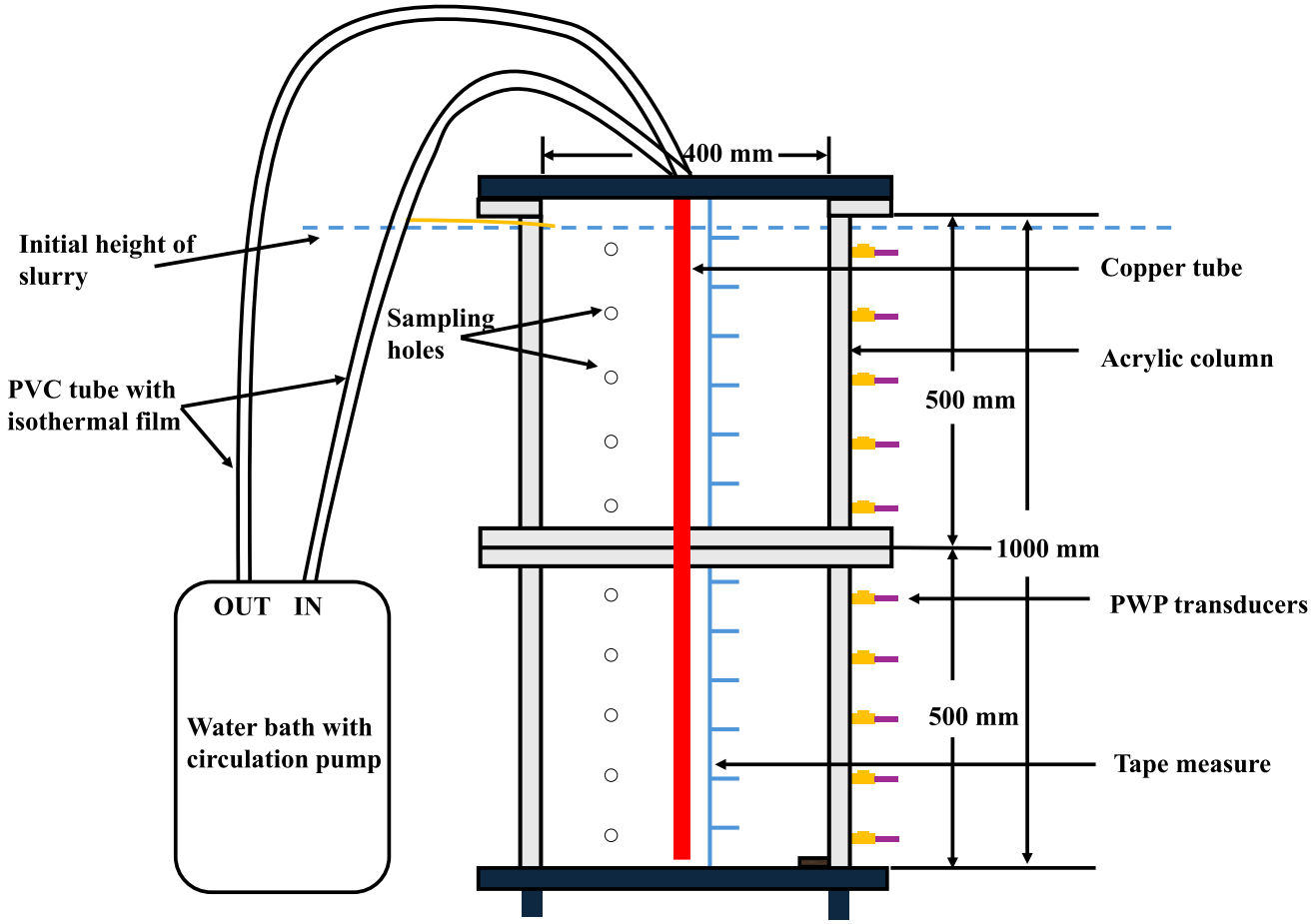

Fig. 5 Schematic diagram of the setup of two physical model tests

temperature of 20 °C), while Test 2 was heated to 40 °C at the start of consolidation. In the physical model tests, only the copper pipe carrying circulating hot water was installed along the central axis of the soil, with no horizontal drainage channel (i.e., no PVD installed in the soil). Consequently, when applying the theoretical model derived in this study to simulate this experiment, the boundary at $r = r_w$ should be treated as impermeable; only the top boundary is set as a permeable drainage boundary. Under the combined action of its self-weight and heat preloading, the soil undergoes consolidation settlement. Test 1 ran for 180 days, while Test 2 lasted 122 days. During each test, a high-resolution camera was used to track the settlement of HKMD showing on a tape measure. Based on the recorded settlements, time at the end of the primary consolidation (t_{eop}) for Test 1 is approximately 38.6 days, while for Test 2 it is around 23.7 days.

Referring to Liu et al. [26], the void ratio used was obtained indirectly through water content. According to the temperature boundary condition, the coefficients h and h_1 were set as relatively large values, say 1000, to simulate the adiabatic boundary, while the top boundary was a constant temperature boundary, so h_2 was set as a relatively small value (e.g., 0.001). The density of soil particles was measured at 2.63 g/cm^3. The values of expansion coefficients for soil particles and soil skeleton, specific heat capacity of the soil, and coefficient of thermal conductivity were sourced from Liu et al. [26]. The reference time was taken as 1440 min (24 h). Due to the high initial water content, the initial effective stress should be set as a very small value. This value is in the denominator of Eq. (6), which means it cannot be zero; hence, this value could be taken as an identified parameter or set as a small value, such as 0.15 kPa, which is equivalent to placing a feather on a fingernail. Table 3 summarizes the values of the parameters used in the proposed model. The parameters selected for optimization included the hydraulic conductivity $k_{\xi T_0} \in [1 \times 10^{-8}\mathrm{m/s},\ 1 \times 10^{-6}\mathrm{m/s}]$, compression index $\lambda \in [0.5,\ 2]$, permeability index $C_{k\xi} \in [0.5,\ 1.5] \times \lambda \cdot \ln 10$, virgin heating compression index $\lambda_T \in [0.1,\ 7]$, and creep coefficient $\psi \in [0.03,\ 0.08] \times \lambda$.

To balance the calculation efficiency and precision, the swarm size and maximum number of iterations in the PSO algorithm were taken as 30 and 50 for different observed

Table 3 Partial parameters used in the proposed model

Parameter	Value	Unit
r_e	0.2	m
r_w	0.075	m
α_s	3×10^{-5}	1/°C
α_w	2.08×10^{-4}	1/°C
α_u	5.2×10^{-5}	1/°C
ρ_{sT_0}	2.63	g/cm^3
ρ_{wT_0}	0.998	g/cm^3
λ_s	2.5	W/m/°C
λ_w	0.6	W/m/°C
C_s	730	J/kg/°C
C_w	4186	J/kg/°C
C_{kr}	$C_{k\xi}$	–
h	1000	–
h_1	1000	–
h_2	0.001	–
κ	$\lambda/5$	–
κ_T	$\lambda_T/5$	–
e_0	9.5	–
σ'_{zp0}	0.15	kPa
t_0	1440	min

Table 4 Optimized parameters calculated from different observation times

Parameter	Observed time/days			Unit
	10	30	50	
$k_{\xi T_0}$	1.8466×10^{-8}	2.1087×10^{-8}	2.092×10^{-8}	m/s
λ	1.4979	1.4994	1.5	–
$C_{k\xi}$	$1.5 \cdot \lambda \cdot \ln 10$	$1.5 \cdot \lambda \cdot \ln 10$	$1.5 \cdot \lambda \cdot \ln 10$	–
ψ	0.03λ	0.0314λ	0.03λ	–
λ_T	6.9965λ	6.997λ	7λ	–

times, respectively. The selection process of these two parameters will be illustrated in Sect. 5. The calculation procedures for obtaining the optimized parameters are performed on a personal computer equipped with a Windows 11 operating system, an Intel(R) Core(TM) i9-14900HX CPU running at 2.2 GHz, 32 GB of memory, and a 1 TB SSD. The CPU calculation time for three different optimized procedures listed in Table 4 is 6.5321 h, 7.8806 h, and 11.1612 h, respectively.

As mentioned above, the primary consolidation times under the two tests were approximately 38.6 days (Test 1) and 23.7 days (Test 2), respectively. Based on these values, three observation windows of 10, 30, and 50 days were selected to assess the PSO-assisted method across increasingly complete stages of consolidation. Specifically, a 10-day window represents a severely truncated dataset, testing whether early-stage measurements alone can yield meaningful parameter estimates. A 30-day window, by contrast, allows evaluation of the PSO-assisted method when observations approach the completion time of primary consolidation. Finally, a 50-day window that surpasses both primary consolidation times and subsequent creep-driven settlements was employed to test the performance of the PSO-assisted method. The fitness function was calculated according to Eq. (12), and the calculation process followed the detailed steps illustrated in Sect. 3. Table 4 summarizes the optimized parameters calculated using the PSO-assisted finite strain thermal consolidation calculation procedure.

Figures 6, 7, and 8 demonstrate the parameter optimization and error convergence behavior of a PSO-assisted method under varying observation durations (10, 30, and 50 days). Each figure comprises six subplots tracking the iteration evolution of hydraulic conductivity, normal compression index, permeability index, creep index, and virgin heating compression index During the iteration process. For 10-day observation (Fig. 6), the parameters converge to stable equilibria within 30 to 40 iterations: $k_{\xi T_0}$ at 1.8466×10^{-8} m/s (Fig. 6a), λ at 1.4979 (Fig. 6b), $C_{k\xi}$ at $1.5 \times \lambda \cdot \ln 10$ (Fig. 6c), ψ at $0.03\ \lambda$ (Fig. 6d), λ_T at 6.9965λ(Fig. 6e). Total error (Fig. 6f) decreases monotonically, demonstrating rapid error suppression. For 30-day observation (Fig. 7), parameter stability improves significantly. Extending the observation to 50 days, optimization efficiency further increases. As shown in Fig. 8, all parameters achieve convergence 20% to 30% faster than in shorter observation time. All the optimization parameters are listed in Table 4. Figures 6f, 7f, and 8f show that for observation times of 10, 30, and 50 days, and the total errors converge to 25.70, 159.24, and 166.00, respectively, yielding mean squared error (MSE) values of 0.41, 1.54, and 1.46 via Eq. (13). That is, an average prediction error per point of less than 1.25 cm. A smaller MSE at the shorter (10-day) observation interval arises simply because fewer data points dilute the accumulated error. However, this does not mean superior model performance is reached, since dividing a small total error by a small sample size can produce a lower per-point average.

Figure 9 shows the calculation results using the optimized parameters listed in Table 4 under two temperatures (i.e., 20 °C in Test 1 and 40 °C in Test 2) and three different observation times. It can be seen from the figure that time t is divided into two parts, the first part named Stage 1 is used in the PSO-assisted method for searching the undetermined parameters, while the second part named

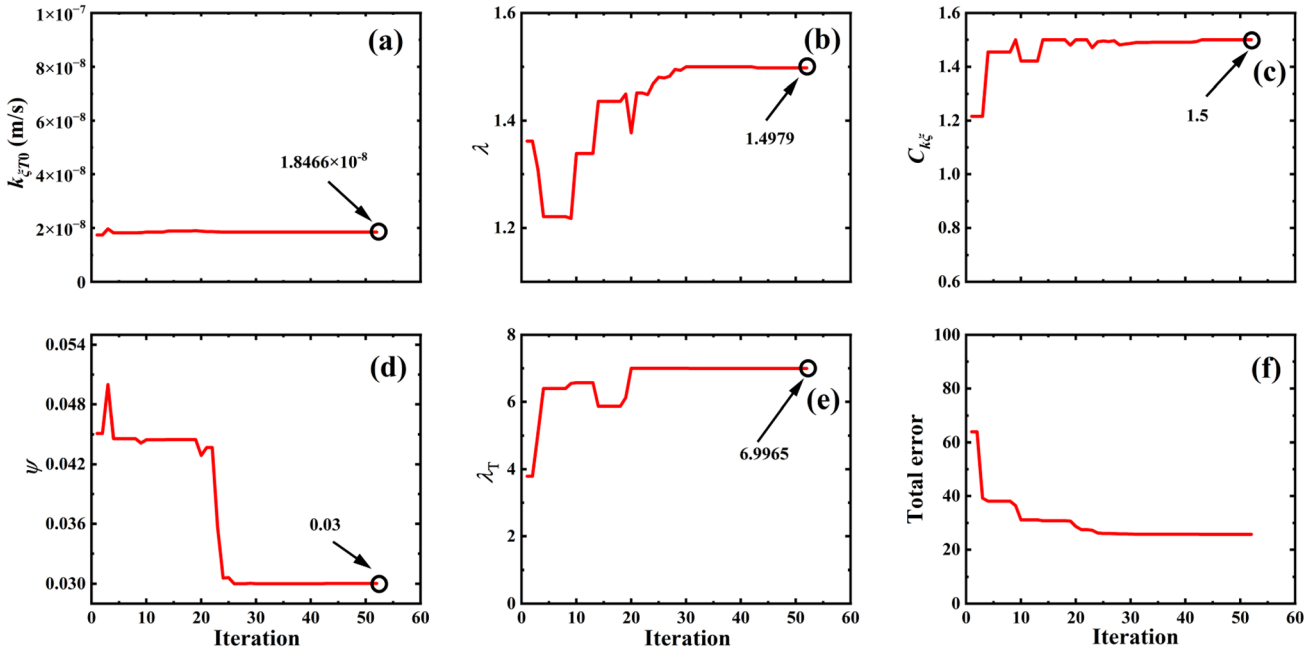

Fig. 6 Optimization parameters and total error calculated using PSO-assisted method with the observed time of 10 days

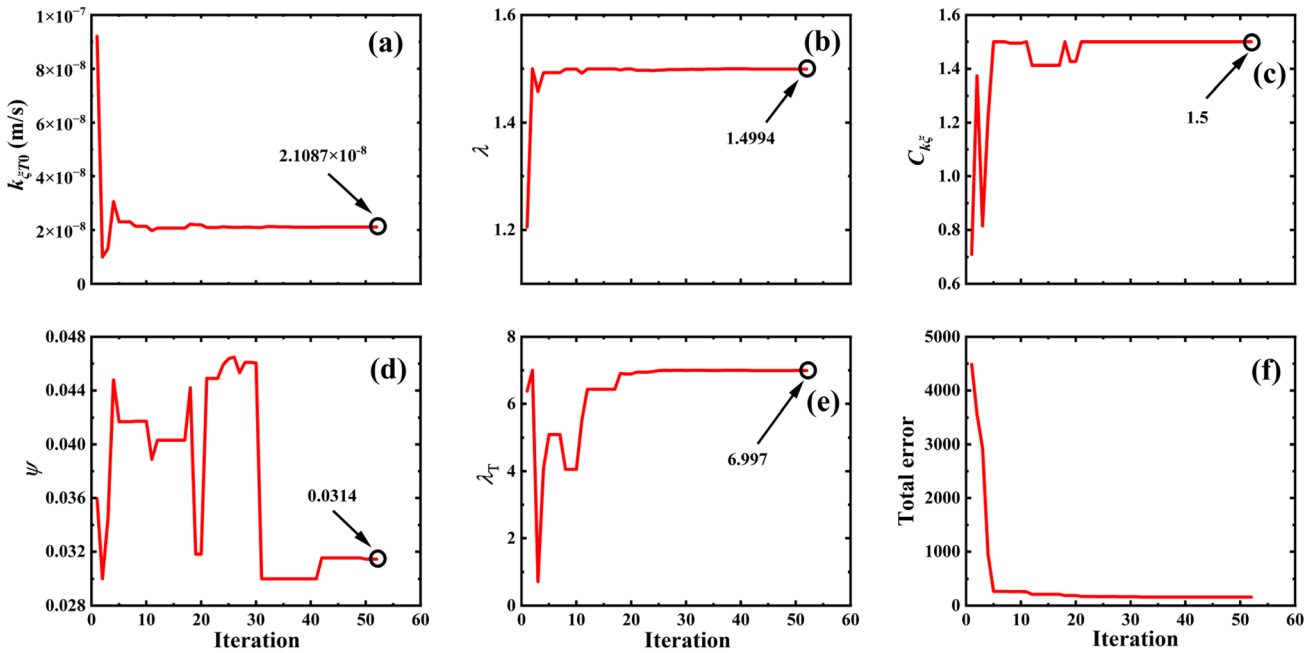

Fig. 7 Optimization parameters and total error calculated using PSO-assisted method with the observed time of 30 days

Stage 2 is employed to examine the predictive capacity. As shown in Fig. 9, when the observed time is taken as 10 days, a pronounced difference (at least larger than 11%) has been found in the subsequent prediction process, and the larger the value of observed time, the smaller the difference in observed and measured data, the better the predictive effects. Limited observational data may contain inherent noise and fail to comprehensively characterize the nonlinear finite strain thermo-consolidation behavior. Extending observation periods mitigates the impact of noise while accentuating the distinctive features of nonlinear consolidation, allowing mathematical models to better capture these changes. Consequently, the PSO-assisted method achieves higher efficiency in parameter optimization and presents improved predictive accuracy. Even though predicted settlements calculated by the

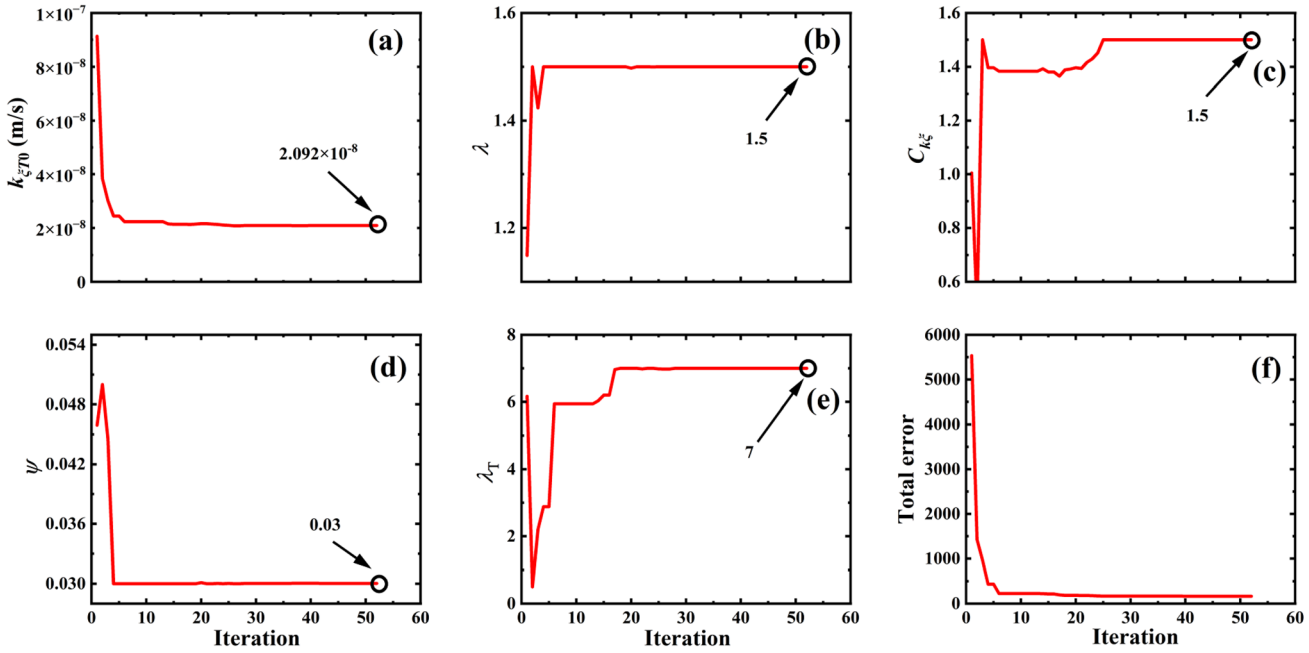

Fig. 8 Optimization parameters and total error calculated using PSO-assisted method with the observed time of 50 days

optimized parameters obtained from a shorter observed time (e.g., 10 days) may not have a good prediction of a large time range, the subsequent few days' predictions, say 2 or 3 days, can still provide a reasonable reference. By obtaining and introducing more observed settlement data, such as 30 days (see Fig. 9a) or 50 days (see Fig. 9b), the predicted settlement curve gradually aligns with real-world measurements. Therefore, it can be concluded that the more monitoring data the algorithm incorporates, the higher its accuracy becomes. Moreover, the observed data show viscous characteristics (refer to creep deformation here), which have been captured by the proposed model. Therefore, considering the viscous characteristics of soft soils is meaningful. Although there remains a deviation between the predicted curves and measured data During Stage 2, with the proposed model appearing to slightly overestimate measured settlement when the observation time is 30 days or longer, this error is minor (below 4%, see Fig. 10c) and is expected to decrease as additional observation points are incorporated.

To quantify the predictive effects, two indices, namely MSE and relative error (RE), are employed to evaluate the capacity. The square mean error and relative error are defined as:

$$\mathrm{MSE} = \frac{1}{n}\sum_{i=1}^{n}(s_i - \hat{s}_i)^2$$
$$\mathrm{RE} = \frac{s_i - \hat{s}_i}{s_i} \times 100\% \tag{13}$$

where s_i is the ith observed settlement value and $\hat{s}_i$ is the ith predicting settlement value.

Figure 10a to 10c displays scatter plots that compare predicted and observed settlement at two temperature conditions (i.e., 20 °C and 40 °C). Figure 10a illustrates that the predicted settlement values at 20 °C (blue squares) closely align with the observed data along the optimum prediction line (dashed line), resulting in a minimal relative error of 7.99%. Predicted settlements at 40 °C (red dots) show increased deviations, with a maximum relative error of 19.54%. Figure 10b illustrates enhanced precision at both temperatures, with relative error diminished to 5% (40 °C) and 3.88% (20 °C). The small range in Fig. 10c reaches nearly ideal accuracy, with errors as minimal as 1.69% (20 °C) and 3.54% (40 °C). Besides, the overall MSE (i.e., a combination of MSE in different temperatures during Stage 2 period) during Stage 2 period, calculated using Eq. (13) for three different observed times, is 3.0993, 0.2877, and 0.2705, respectively. The quantified error analysis further emphasizes that when the chosen observation period is equal to or greater than the primary consolidation completion time, the error of Stage 2 falls below 5%. Therefore, to achieve high-accuracy predictions, the observation window should be no shorter than the time required for primary consolidation. Moreover, in practical applications of the present model combined with the PSO-assisted method, monitoring data collected continuously after the primary consolidation period could be incorporated to further enhance prediction accuracy.

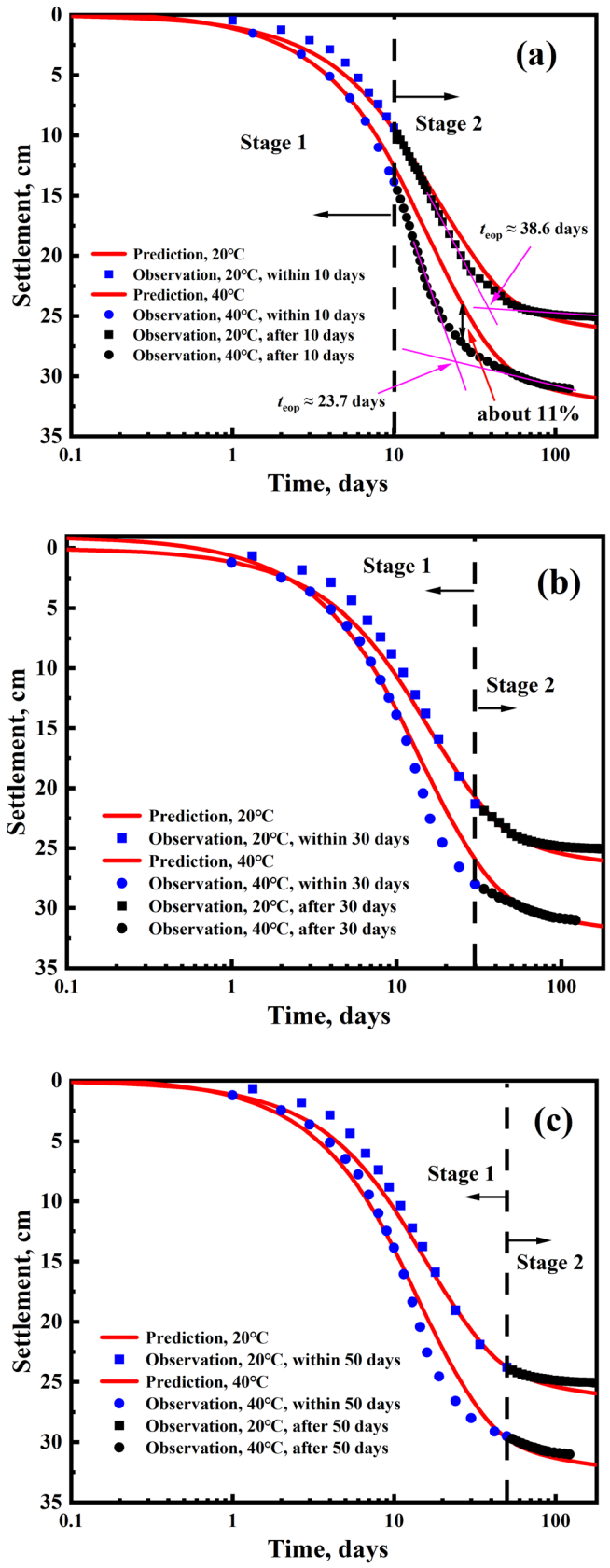

Fig. 9 The comparison of settlement between the experimental data and predicted values with different observed times: **a** 10 days, **b** 30 days, and **c** 50 days

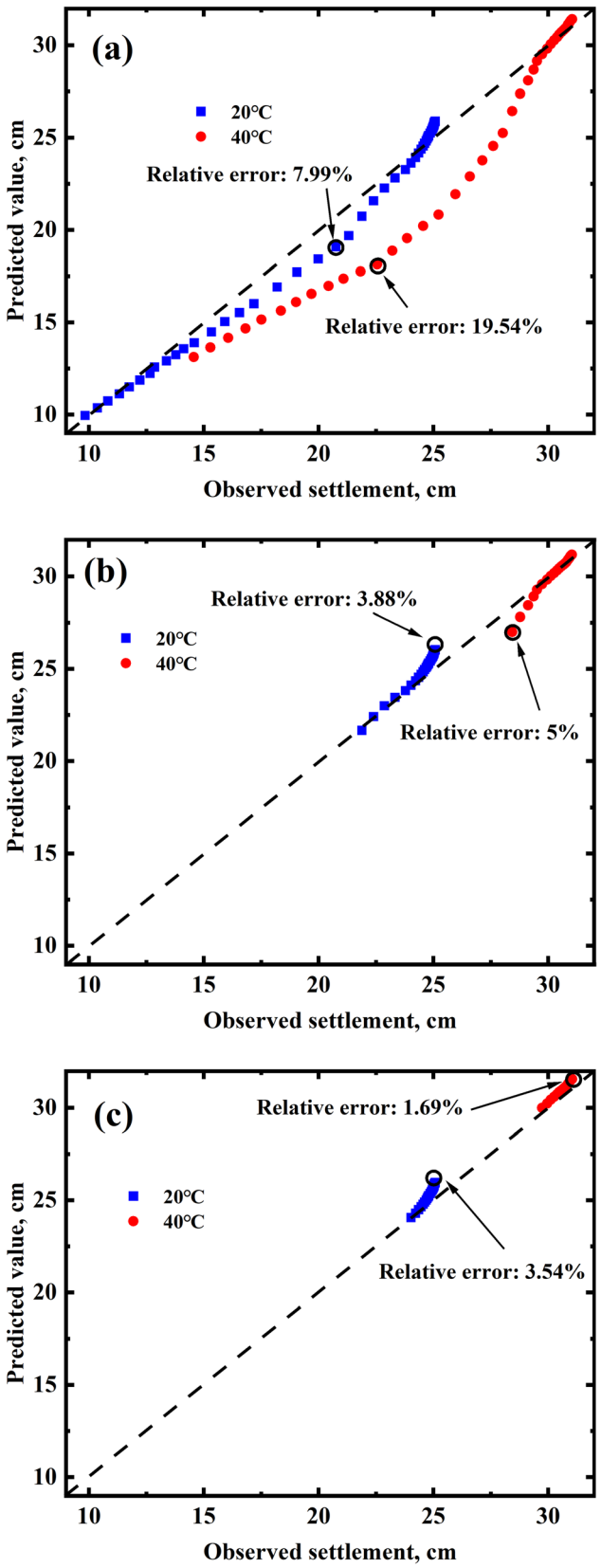

Fig. 10 Scatter plots of predicted and observed settlements with different observed times: **a** 10 days, **b** 30 days, and **c** 50 days

5 Selection of PSO algorithm parameters

The selection of PSO parameters, particularly the swarm size and maximum iteration numbers, significantly impacts the computation of optimized parameters and, as a result, affects the predictive capability of a prediction model. Optimal settings must achieve a balance between estimation accuracy and computational cost. A swarm size and maximum iteration numbers that are too small can result in unstable searches and biased fits. Conversely, excessively large values may enhance precision but significantly increase the runtime.

A universal combination of swarm size and maximum iteration numbers may not exist. Two practical strategies are commonly recommended. One approach is to ignore calculation costs and utilize significantly large values (e.g., swarm size = 100 and maximum iteration numbers = 100 as referenced in [5]), which demonstrates robustness but lacks efficiency. This study adheres to a more cost-effective protocol. The swarm size is initially selected from the recommended range of 20–40 [30], with a fixed size of 30 in this paper. Subsequently, the maximum number of iterations is increased until convergence is achieved for both the total error function and the optimized parameters. The data provide evidence that supports this choice. Table 5 presents a comparison of three sets of PSO algorithm parameter combinations, namely, combination I, combination II, and combination III, and the corresponding swarm sizes and maximum iteration numbers for these combinations are (10, 30), (30, 50), and (50, 70), respectively. The computation duration increases markedly from 1.6415 h for combination I to 7.8806 h for combination II and thereafter to 20.1054 h for combination III. Notably, the optimized parameters for combination II and combination III are almost identical. The convergence histories presented in Fig. 11 demonstrate that the total loss and optimized parameter estimates converged after approximately 45 iterations. Figure 12 consistently demonstrates that the predicted settlement curves for combinations II and III are nearly identical, while combination I exhibits a significant deviation. Based on this analysis, we select 30 as the swarm size and 50 as the maximum number of iterations. The selected parameter combination ensures quick and stable convergence, avoiding the diminishing returns associated with larger swarms or increased iteration numbers.

Increasing the number of observation points results in a higher cost for each fitness evaluation, as each particle must be assessed against a greater volume of data. However, this adjustment does not change the dimensionality of the optimized parameter space. Therefore, the swarm size and maximum iteration numbers typically do not require

Table 5 Optimized parameters calculated from different sets of PSO algorithm parameter combinations

Parameter	Different PSO algorithm parameter combinations			Unit
	I	II	III	
$k_{\xi T_0}$	2.4790×10^{-8}	2.1087×10^{-8}	2.1020×10^{-8}	m/s
λ	1	1.4994	1.4999	–
$C_{k\xi}$	$1.5 \cdot \lambda \cdot \ln 10$	$1.5 \cdot \lambda \cdot \ln 10$	$1.5 \cdot \lambda \cdot \ln 10$	–
ψ	0.0314λ	0.0314λ	0.0315λ	–
λ_T	7λ	6.997λ	6.999λ	–

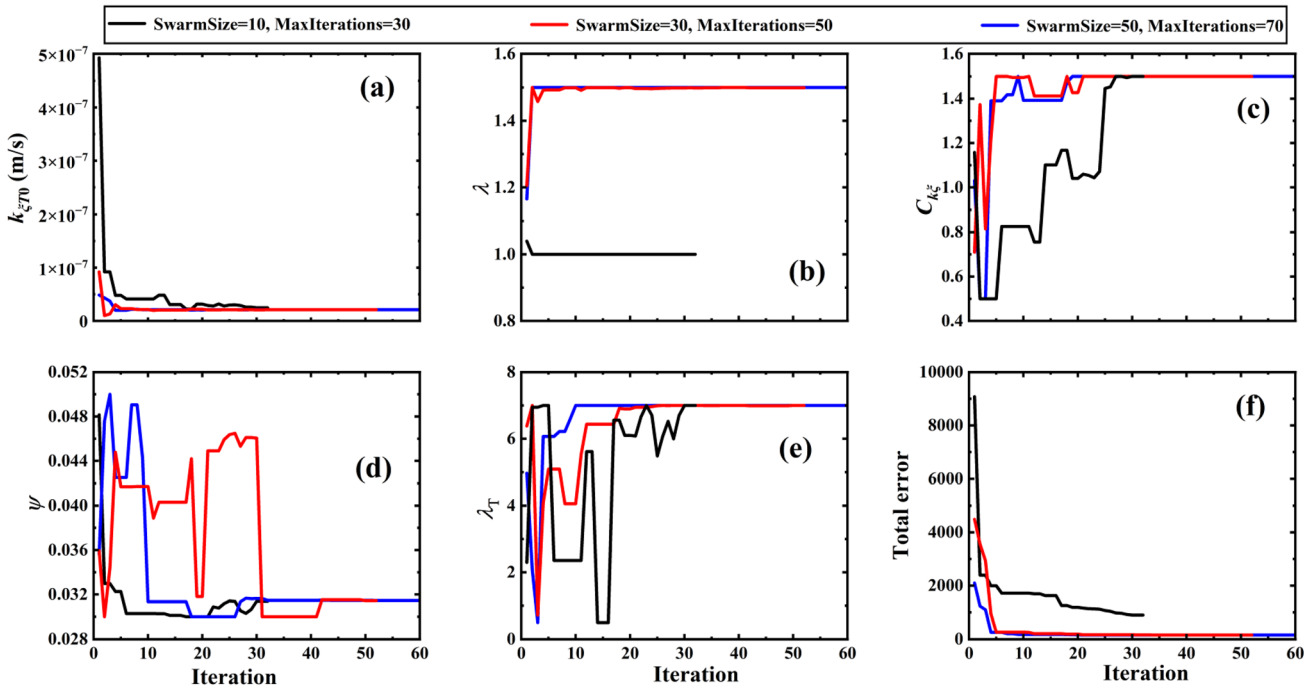

Fig. 11 Optimization parameters and total error calculated from three sets of PSO algorithm parameter combinations with the observed time of 30 days

changing when the dataset is extended. The results from our experiments demonstrate that, when utilizing consistent settings (swarm size = 30, maximum iteration numbers = 50), the 50-day observations yielded stable parameter estimates and a converged loss. This confirms the effectiveness of our selected PSO algorithm parameters across varying data lengths without compromising performance (refer to Fig. 8).

6 Conclusions

The main conclusions of this paper are summarized as follows:

(1) A radial finite strain consolidation model incorporating thermal elastic visco-plastic constitutive model is extended to further consider the viscous behavior of soft soils. A numerical solver has been employed to solve the coupled governing equations. Two verification cases have been conducted to verify the correctness of the numerical solution method.

(2) A PSO-assisted method has been proposed to enhance the performance of the proposed consolidation model. This algorithm combines the established consolidation model, limited observed data, and results from conventional techniques to conduct real-time accurate prediction of thermal consolidation behavior for soft soils.

(3) Two physical model tests have been performed to examine the validity of the proposed consolidation model as well as the PSO-assisted analysis method. The comparison between the test and calculation results highlights the necessity of establishing the newly developed consolidation model and the usefulness of the proposed algorithm.

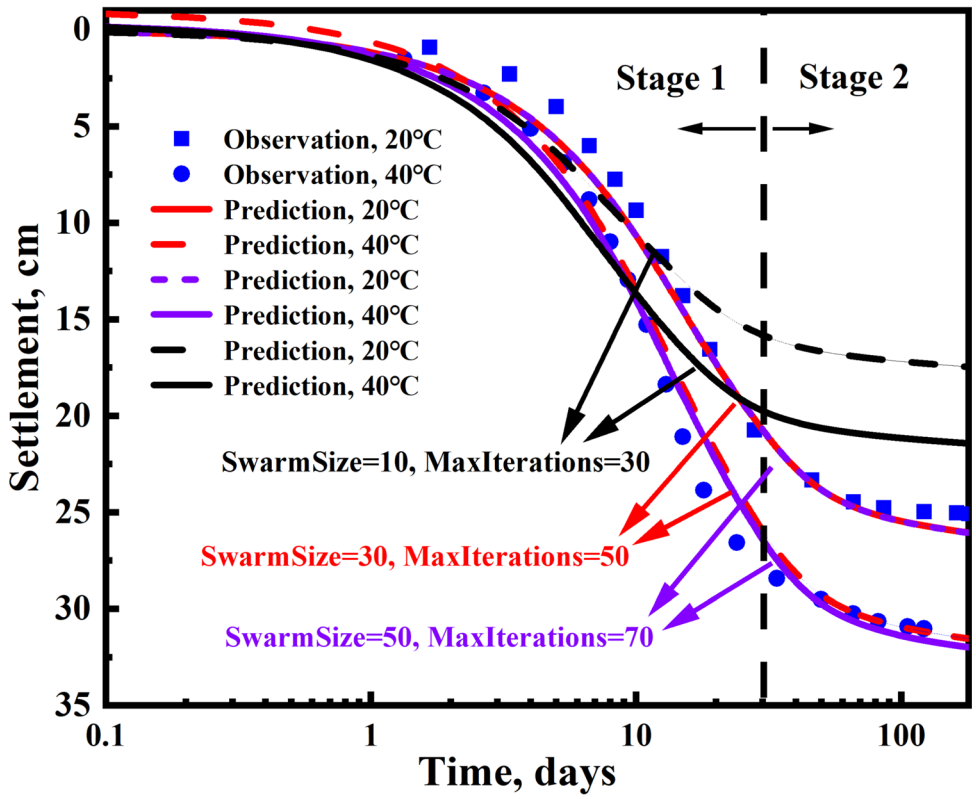

Fig. 12 The comparison of settlement between experimental and predicted values calculated from three sets of PSO algorithm parameters combination when the observed time of 30 days

(4) For field-scale applications of the proposed consolidation model, it is recommended that the observation dataset should include primary consolidation measurements to ensure high accuracy of subsequent predictions. Additionally, even when predictions are based on observation times beyond primary consolidation, practical application of the present model with the PSO-assisted method can incorporate monitoring data collected after the primary consolidation period to further improve forecast accuracy During Stage 2.

(5) The determination of swarm size and maximum iteration numbers in the PSO algorithm typically involves two methods. One option for the swarm size is to select a range between 20 and 40. The minimum number, or any number above this threshold, that ensures the convergence of optimized parameters and the loss function can be regarded as the maximum number of iterations. In contrast, two big values, such as 100 and 100, can be selected for swarm size and maximum iteration numbers without considering computational costs.

Acknowledgements The work presented in this paper is supported by the Research Grants Council (RGC) of Hong Kong Special Administrative Region Government (HKSARG) of China (GRF: 15210020, 15221721, and 15226722). The work is also supported by the Natural Science Foundation of Wuhan (No.2024040801020271) and Fundamental Research Funds for Central Public Welfare Research Institutes of China (No. CKSF20241004/YT). The authors also acknowledge the financial support from three grants (CD7A and CD7J) from Research Institute for Land and Space, a postdoctoral matching fund scheme (W314), and a start-up fund (BD30) of The Hong Kong Polytechnic University.

Funding Open access funding provided by The Hong Kong Polytechnic University.

Data availability All data, models, or code that support the findings of this study are available from the corresponding author upon reasonable request.

Declarations

Conflict of interest The authors declare that there is no conflict of interest regarding the publication of this paper.

References

1. Abuel-Naga HM, Bergado DT, Bouazza A, Ramana GV (2007) Volume change behaviour of saturated clays under drained heating conditions: experimental results and constitutive modeling. Can Geotech J 44(8):942–956
2. Abuel-Naga HM, Bergado DT, Bouazza A, Pender M (2009) Thermomechanical model for saturated clays. Geotechnique 59(3):273–278
3. Ahmadi-Nedushan B, Varaee H (2009) Optimal design of reinforced concrete retaining walls using a swarm intelligence technique. In: The first international conference on soft computing technology in civil, structural and environmental engineering, UK
4. Chai JC, Carter JP, Hayashi S (2005) Ground deformation induced by vacuum consolidation. J Geotech Geoenviron Eng 131(12):1552–1561
5. Chen P, Wang B, Ma K (2025) Optimal design and numerical studies of negative stiffness device–TMD controlled systems using PSO algorithm. Soil Dyn Earthq Eng 189:109111
6. Chen Z-J, Yin J-H (2023) A new one-dimensional thermal elastic-viscoplastic model for the thermal creep of saturated clayey soils. J Geotech Geoenviron Eng 149(4):04023010
7. Chen Z-J, Feng W-Q, Chen W-B, Yin J-H (2023) A thermal elastic visco-plastic model for soft clayey soils. Can Geotech J 61(2):208–227
8. Chen Z-J, Feng W, Li A, Al-Zaoari KYM, Yin J-H (2023) Experimental and molecular dynamics studies on the consolidation of Hong Kong marine deposits under heating and vacuum preloading. Acta Geotech 18(5):2569–2583
9. Cheng YM, Li L, Chi S-C, Wei WB (2007) Particle swarm optimization algorithm for the location of the critical non-circular failure surface in two-dimensional slope stability analysis. Comput Geotech 34(2):92–103
10. Chu J, Yan SW, Yang H (2000) Soil improvement by the vacuum preloading method for an oil storage station. Geotechnique 50(6):625–632
11. Chu J, Bo MW, Choa V (2006) Improvement of ultra-soft soil using prefabricated vertical drains. Geotextiles Geomembr 24(6):339–348
12. Cui YJ, Sultan N, Delage P (2000) A thermomechanical model for saturated clays. Can Geotech J 37(3):607–620
13. Du C, Hu X, Fu H, Wang J (2021) Effects of temperature circulation on dredged sludge improved by vacuum preloading. Soils Found 61(5):1343–1353
14. Fox PJ, Nicola MD, Quigley DW (2003) Piecewise-linear model for large strain radial consolidation. J Geotech Geoenviron Eng 129(10):940–950
15. Geng X, Yu H-S (2017) A large-strain radial consolidation theory for soft clays improved by vertical drains. Geotechnique 67(11):1020–1028
16. Heins E, Grabe J (2017) Class-A-prediction of lateral pile deformation with respect to vibratory and impact pile driving. Comput Geotech 86:108–119
17. Hueckel T, Borsetto M (1990) Thermoplasticity of saturated soils and shales: constitutive equations. J Geotech Eng 116(12):1765–1777
18. Indraratna B, Zhong R, Fox PJ, Rujikiatkamjorn C (2017) Large-strain vacuum-assisted consolidation with non-Darcian radial flow incorporating varying permeability and compressibility. J Geotech Geoenviron Eng 143(1):04016088
19. Kashani AR, Gandomi M, Camp CV, Gandomi AH (2020) Optimum design of shallow foundation using evolutionary algorithms. Soft Comput 24:6809–6833
20. Kennedy J, Eberhart R (1995) Particle swarm optimization. In: Proceedings of ICNN'95-international conference on neural networks, Ieee, pp 1942–1948
21. Laloui L, Cekerevac C (2003) Thermo-plasticity of clays: an isotropic yield mechanism. Comput Geotech 30(8):649–660
22. Lambe TW (1973) Predictions in soil engineering. Geotechnique 23(2):151–202
23. Li A, Chen Z-J, Feng W-Q, Yin J-H (2023) The effects of temperature on one-dimensional consolidation and creep behaviors of Hong Kong marine deposits. Int J Geomech 23(12):04023215
24. Li P, Yin J-H, Yin Z-Y, Chen Z (2023) One–dimensional nonlinear finite strain analysis of self–weight consolidation of soft clay considering creep. Comput Geotech 153:105081
25. Liu Y, Wu P-C, Li P-L, Yin J-H, Zheng J-J (2024) Fully coupled large-strain radial consolidation analysis for dredged marine slurry treated by prefabricated vertical drain with vacuum and heat preloading. Comput Geotech 177:106852
26. Liu Y, Li A, Wu P-C, Li P-L, Yin J-H, Zheng J-J (2025) Fully coupled finite strain consolidation analysis for soft clay treated by prefabricated horizontal drain with vacuum and heat preloading. Can Geotech J 62:1–19
27. Losacco N, Viggiani GM (2019) Class A prediction of mechanised tunnelling in Rome. Tunn Undergr Sp Technol 87:160–173
28. Lu M, Sun J, Wen M, Yang K, Li K (2025) Insight into nonlinear thermal consolidation of saturated clay under coupled thermo-mechanical loading: a unified one-dimensional model. Acta Geotech 20:641–667
29. Ng CWW, Zhao X, Zhang S, Zhang Q (2024) A unified thermo-mechanical bounding surface model for saturated clay and sand. Comput Geotech 173:106535
30. Poli R, Kennedy J, Blackwell T (2007) Particle swarm optimization: an overview. Swarm Intell 1(1):33–57
31. Pothiraksanon C, Bergado DT, Abuel-Naga HM (2010) Full-scale embankment consolidation test using prefabricated vertical thermal drains. Soils Found 50(5):599–608
32. Samarakoon RA, McCartney JS (2023) Simulation of thermal drains using a new constitutive model for thermal volume change of normally consolidated clays. Comput Geotech 153:105100
33. Samarakoon RA, Kreitzer IL, McCartney JS (2022) Impact of initial effective stress on the thermo-mechanical behavior of normally consolidated clay. Geomech Energy Environ 32:100407
34. Saowapakpiboon J, Bergado DT, Thann YM, Voottipruex P (2009) Assessing the performance of prefabricated vertical drain with vacuum and heat preloading. Geosynth Int 16(5):384–392
35. Shi L, Wang Q-Q, Xu S-L, Pan X-D, Sun H-L, Cai Y-Q (2018) Numerical study on clogging of prefabricated vertical drain in slurry under vacuum loading. Granul Matter 20(4):74
36. Yin J-H, Graham J (1994) Equivalent times and one-dimensional elastic viscoplastic modelling of time-dependent stress–strain behaviour of clays. Can Geotech J 31(1):42–52
37. Zhou Y-D, Wu S-L, Wang Z-X, Guo S-J (2024) Large strain radial thermo-consolidation model for saturated soil foundation. Comput Geotech 176:106788